RESEARCH ARTICLE

Macromolecular Materials and Engineering
Open Access
www.mame-journal.de

High-Throughput Electrospinning of Unmodified and Aminated Poly(Pentafluorostyrene) for Fiber-Reinforced Proton Exchange Membranes

Muhammad Solihul Mu'min, Anja Krieger,* Maximilian Wagner, Simon Thiele, and Jochen Kerres*

This study demonstrates a high-throughput fabrication of fiber interlayers for proton exchange membranes based on poly(pentafluorostyrene) (PPFSt) and its aminated derivatives. The fibers are produced by electrospinning, where the parameters are carefully screened. The controlled parameters are solvent composition, weight percentage, voltage, flow rate, and temperature, controlled with a self-designed heating jacket. The parameters are iterated toward optimized fiber structure and maximum output. The yielded fibers are infiltrated with Nafion and sulfonated polymer from bisphenol AF and decafluorobiphenyl (SFS001) by spray-coating and doctor blading to obtain the fiber-reinforced proton exchange membranes. Tensile tests reveal a higher Young's modulus and yield stress than pure Nafion. Here, the basicity of the aminated PPFSt fibers correlates with the Young's modulus due to improved acid-base interactions between amine groups and sulfonic acid. The acid-base interactions influence the composite membrane's proton conductivity, varying from 23 mS cm^{-1} for strongly alkaline fibers to 69 mS cm^{-1} for non-basic fibers. These findings can be transferred to fabricating fiber reinforcements beyond routinely used poly(benzimidazoles).

1. Introduction

Nanofibers are among the most reported functional structures utilized in numerous applications, including composite membranes in electrochemical energy devices such as fuel cells, electrolyzers, and redox flow batteries.[1] The trend toward using thin membranes encourages applying reinforcement structures to increase the membrane's mechanical stability and control the membrane's permeability.[2,3] In addition, they possess high uniaxial conductivity, which promotes their implementation as a through-plane reinforcement.[4] Different methods, such as centrifugal spinning, wet spinning, melt spinning, emulsion spinning, and electrospinning, can be utilized to carry out the fiber preparation. Electrospinning is considered the most scalable, affordable, and functional method to produce nanofibers from various material types, such as polymers, metals, ceramics, and carbons.[5]

In electrospinning, nanofibers can be generated with various shapes, such as belts and spindles with varying diameters.[6] Ideally, fiber-reinforced composites require nanofibers with a high specific surface area to improve the fiber-matrix contact.[7] In this case, the influence of the solvent is the main factor that controls the fiber topology.[8] Besides reducing the nanofiber diameter, fabricating nanofibers with unique surface structures can increase fiber roughness and surface area, improving the adhesion between the fiber and the matrix. Intuitively, for creating such a wide range of fiber properties, multiple parameters can be considered for this process, which can be grouped roughly into solution, process, and environmental parameters, influencing the quality of electrospun nanofibers.[9]

Recently, we developed electrospun nanofibers based on polypentafluorostyrene (PPFSt). This demonstrates a promising polymer reinforcement due to its good mechanical strength, thermal stability, and overall chemical modifiability. However, PPFSt fibers interact poorly with the Nafion matrix, leading to fiber-matrix delamination.[10]

Aminated polymers could circumvent the interaction mismatch with Nafion by ion-pair formation via protonation of the amino group to overcome the incompatibility.[11] This

M. S. Mu'min, A. Krieger, M. Wagner, S. Thiele, J. Kerres
Forschungszentrum Jülich GmbH
Helmholtz Institute Erlangen-Nürnberg for Renewable Energy (IET-2)
Cauerstr. 1, 91058 Erlangen, Germany
E-mail: j.kerres@fz-juelich.de; anja.krieger@fau.de
M. S. Mu'min, S. Thiele
Department of Chemical and Biological Engineering
Friedrich-Alexander-Universität Erlangen-Nürnberg
Egerlandstr. 3, 91058 Erlangen, Germany
J. Kerres
Chemical Resource Beneficiation Faculty of Natural Sciences
North-West University
Potchefstroom 2520, South Africa

The ORCID identification number(s) for the author(s) of this article can be found under https://doi.org/10.1002/mame.202400078

DOI: 10.1002/mame.202400078

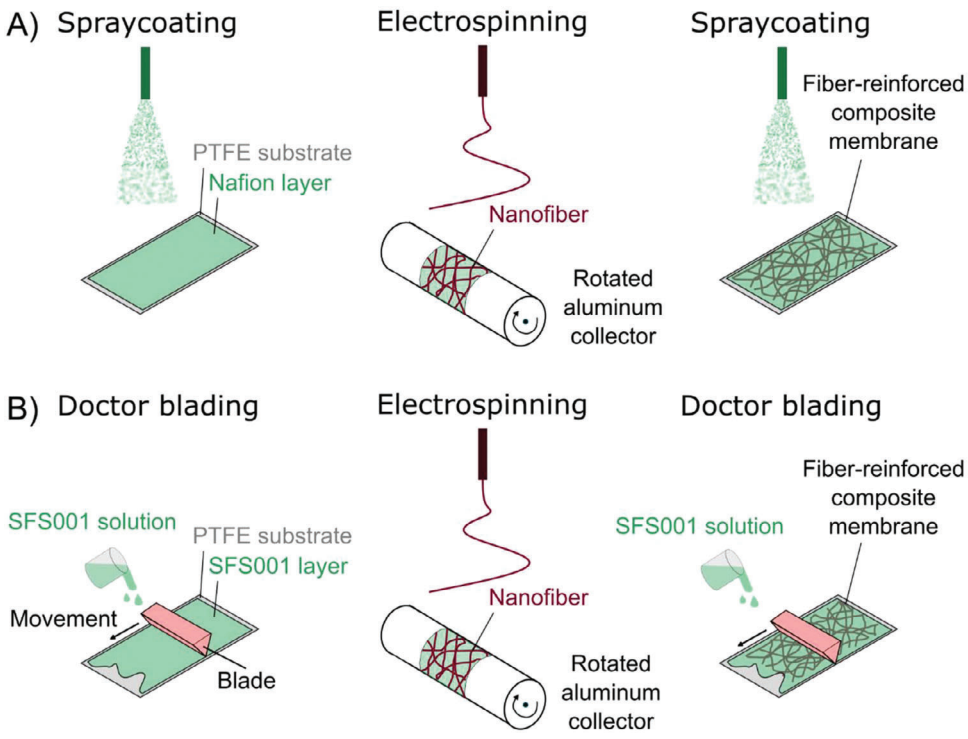

Scheme 1. Fiber-reinforced composite membranes are prepared by two different pore-filling methods: A) includes the spray-coating of a bottom layer of Nafion on a PTFE substrate. In a second step, the PPFSt fibers were deposited by electrospinning on the Nafion bottom layer. The final step includes infiltration of the fibers with Nafion solution creating a symmetric membrane with the fiber mat in its center. B) includes the doctor blading of the SFS001 bottom layer, deposition of PPFSt fibers via electrospinning, and finally, infiltration of the fibers with SFS001 solution forming the symmetric membrane.

concept has been successfully demonstrated by incorporating poly(benzimidazoles) (PBI) as either nanofiber or matrix with a cation-exchange polymer to create an ionically crosslinked fiber-matrix interface, which gains the chemical and mechanical stability of the polymer composite.[12,13] However, producing PBI nanofibers via electrospinning is comparably time-consuming due to the slow flow rate of 0.3–0.5 ml h^{-1} also using multiple needle setups.[14] Other polymers, such as poly(vinylidenefluoride)-(hexafluoropropene), can be electrospun with much higher flow rates of up to 1.8 ml h^{-1}.[15] Hence, preparing aminated polymers from different polymer backbones, such as PPFSt, can enable high throughput in preparing electrospun fibers while maintaining beneficial solid interactions between the fibers and the matrix.

In this work, the parameters for the high-throughput production of PPFSt fibers were optimized by varying the crucial electrospinning parameters. This knowledge was transferred to the electrospinning of tetramethylguanidine (TMG) and piperidine (Pip) functionalized PPFSt in the second step. Scanning electron microscopy (SEM) was used to study the effect of the electrospinning parameters as well as the effect of amination of the PPFSt. Further, the fibers were infiltrated with Nafion and sulfonated polymer from bisphenol AF and decafluorobiphenyl (SFS001),[16] respectively, to yield the composite proton exchange membranes. The preparation of the complete fiber-reinforced membranes is depicted in **Scheme 1**. For the deposition of Nafion, spray-coating was used (Scheme 1A), whereas, for the deposition of SFS001, doctor blading could be used (Scheme 1B) due to improved handling of the SFS001 solution, compared to Nafion dispersions.

The fiber-reinforced composite membranes were characterized by their mechanical strength, water uptake, and conductivity.

2. Results and Discussion

2.1. Polymer Characterization

The thermo-physical properties of PPFSt and aminated PPFSt are depicted in **Table 1**. Functionalization of PPFSt with the amino group increased the glass transition and thermal decomposition temperature. The glass transition temperature (T_g) for PPFSt-Pip is 146.97 °C, significantly higher than that of PPFSt at 109.68 °C, while PPFSt-TMG possesses a T_g of 159.50 °C. The reason for the higher T_g of the aminated PPFSt polymers

Table 1. Glass transition temperature (T_g) and thermal decomposition temperature ($T_{decomposition}$) of PPFSt and aminated PPFSt.

Polymer	T_g [°C]	$T_{decomposition}$ [°C]
PPFSt-Pip	146.97	329
PPFSt-TMG	159.50	296
PPFSt	109.68	285[a)]

[a)] Taken from reference [17].

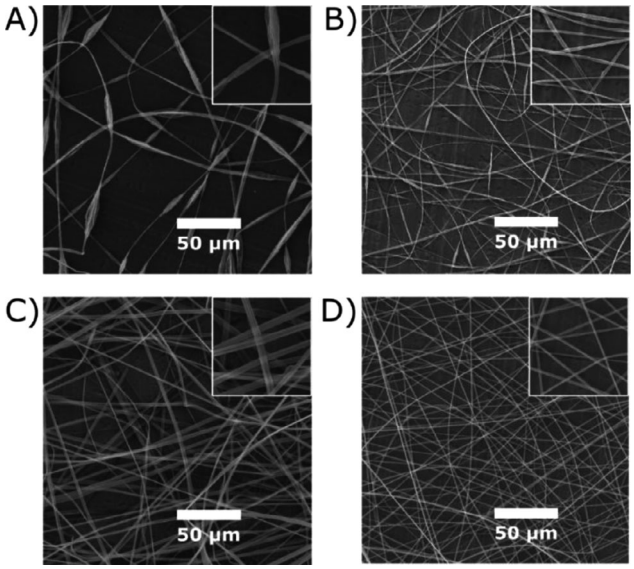

Figure 1. Effect of solvents: A) THF, B) Acetone, C) THF/DMSO (8:2), D) THF/DMAc (1:1). The PPFSt solution concentration is 6 wt.% and electrospun at 10 kV with a flow rate of 2.97 mL h^{-1}.

is the polarity, as TMG provides a lower pK_a value than Pip. From thermogravimetric analysis, the decomposition temperature of PPFSt-Pip achieves the highest value at 329 °C. For PPFSt-TMG and unmodified PPFSt, the decomposition temperatures are comparable at 296 °C (PPFSt-TMG) and 285 °C (PPFSt), respectively. This behavior shows that the attached amino groups influence the decomposition of the backbone, as PPFSt does not provide a functional group and degrades faster under the same conditions.

For rapid screening of the most beneficial parameters for electrospinning, PPFSt is chosen as some of its electrospinning parameters are known from our previous study.[10]

The preparation of the solutions for the different studies and the preparation of the final membranes can be taken from the experimental part. The screening for the ideal parameters for electrospinning was not targeting a specific fiber density yet, focusing on the structural aspect. For the preparation of the later reinforced membranes, a specific fiber density of ≈ 0.65 mg cm^{-2} was targeted, applying the knowledge from the screening experiments for high-throughput fabrication of fibers.

2.2. Effect of Solution Parameters on PPFSt Fiber Morphology

The solution parameters are essential in electrospinning and can significantly impact the output.[18] **Figure 1**A shows the SEM images of electrospun PPFSt-fibers produced from a PPFSt/THF solution. The morphology is not homogeneous, providing multiple spindle structures along the fiber axis. Changing the solvent to acetone yet maintaining the concentration decreases the mean fiber diameter from 1.79 to 1.17 µm and improves the fiber morphology slightly (Figure 1B). Since the surface tension and viscosity of acetone are not significantly different from THF, the improved fiber morphology might originate from the complete polymer solution, where acetone dissolves PPFSt to a different extent than THF. Secondary solvents such as DMAc and DMSO are added to the PPFSt solution to alter the dielectric constant of the solvent. The solvent parameters can be found in Table S1 (Supporting Information). Adding DMAc or DMSO as a secondary solvent into the PPFSt/acetone system produces polymer agglomerates in the solution. However, no agglomeration occurs when DMAc or DMSO are added to the PPFSt/THF solution, and the solution remains transparent for smaller amounts of the high boiling point solvent. For DMAc, up to 50 wt.% DMAc can be added to the PPFSt/THF solution, while DMSO can be added up to 20 wt.%. DMSO, as a secondary non-solvent in the PPFSt/THF solution, improves the fiber structure's homogeneity. At the same time, it increases the mean fiber size to 2.96 µm (Figure 1C) due to its flat shape, which originates from solvent evaporation leaving the exterior polymeric "skin"[19] As for adding DMAc in the PPFSt/THF solution, it significantly improves the electrospinning process and fiber morphology (Figure 1D). The mean fiber diameter produced by adding DMAc decreases to 1.22 µm, and the fiber structure is homogeneous without beads or spindles. To explain these phenomena, a solvent with a larger dielectric constant provides a higher net charge density in the solution. This enhances the jet elongation during electrospinning, reduces the number of beads, and lowers the fiber diameters, as illustrated in the SEM images. A higher content of polar solvent (DMAc) decreases the fiber diameter.

Additionally, THF and acetone used for dissolving PPFSt have low boiling points with 56.2 °C for acetone and 66 °C for THF, causing rapid evaporation during electrospinning. As a result, electrospinning of PPFSt/acetone and PPFSt/THF solutions produces low amounts of fibers before the solidified polymer clogs the nozzle. This renders the electrospinning process inefficient. In theory, a temperature below 0 °C would reduce the evaporation rate. However, this approach is unsuccessful since the PPFSt solution exhibits phase separation at low temperatures.

In **Figure 2**, different fiber morphologies are depicted, resulting from various concentrations of the PPFSt solutions in the same solvent, namely THF/DMAc (1/1). Figure 2A shows the transition of electrospun 2 wt.% PPFSt into solidified droplets accompanied by fibers with a diameter of 400–500 nm. Increasing the PPFSt concentration to 4 wt.% improves the morphology significantly since no beads are identified (Figure 2B). A further increase to 8 wt.% PPFSt creates more homogeneous fibers without beads (Figure 2C). The homogeneous fibers electrospun from 4 and 8 wt.% provide diameters of 0.73 and 1.3 µm, respectively. The PPFSt solution concentration can be increased to more than 20 wt.% PPFSt. However, at higher concentrations, flat fibers with a size of ≈ 8.49 µm wide and an inhomogeneous morphology are generated (Figure 2D).

Droplets are generally obtained for diluted polymer solutions where the macromolecular chains are not entangled sufficiently, leading to Rayleigh instability and subsequently causing bead production.[20] Increasing the polymer concentration improves the polymer entanglement since every polymer chain can merge with its surrounding polymer chains. In addition, the polymer chain entanglement increases the elastic behavior of the polymer jet, overcoming the Rayleigh instability.[9] Besides transforming the droplet into the fiber, increasing polymer concentration can rise adhesion among polymer chains, increasing viscosity. In electrospinning, a polymer jet with higher viscosity hardly elon-

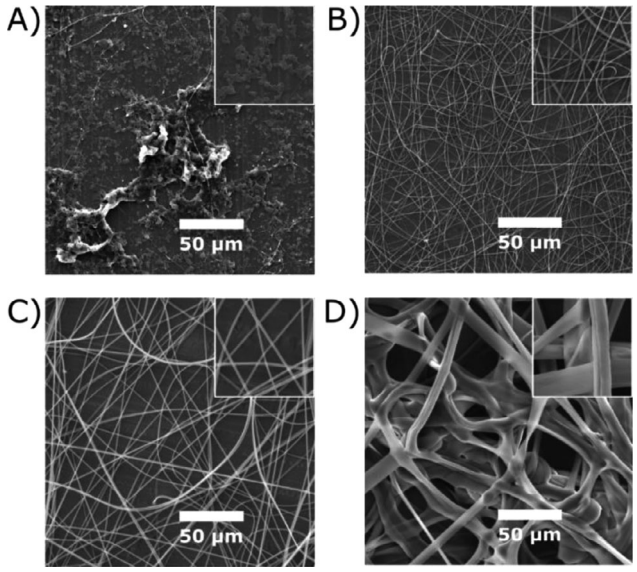

Figure 2. Effect of polymer concentration: A) 2, B) 4, C) 8, and D) 20 wt.%. PPFSt is dissolved in THF/DMAc (1/1). The electrospun PPFSt fibers are produced at 10 kV with a flow rate of 2.97 mL h^{-1}.

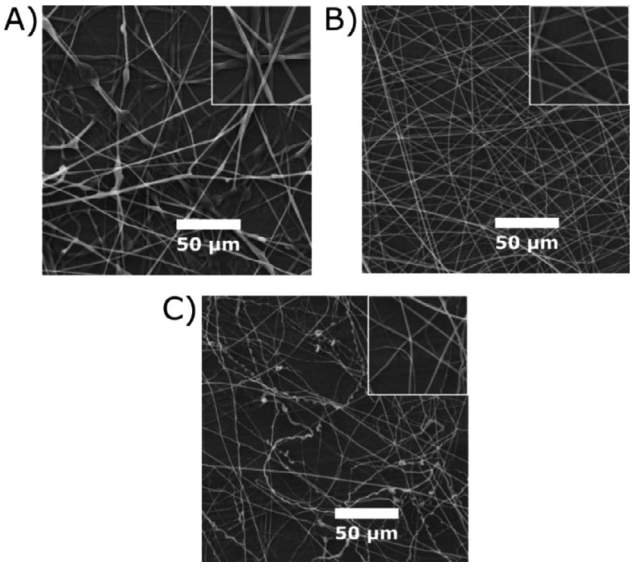

Figure 3. Effect of voltage: A) 7, B) 10,C) 15 kV. The distance between the needle and the collector is 20 cm. The PPFSt solution is dissolved in THF/DMAc (1/1) with a concentration of 6 wt.% and electrospun by setting the flow rate at 2.97 mL h^{-1}.

gates, and the radial stress that shrinks the jet is poor. Consequently, larger fiber diameters are deposited on the collector.

2.3. Effect of operational parameters on PPFSt fiber morphology

The voltage is one of the main parameters behind the production of fiber by electrospinning. A sufficient voltage can induce the polymer solution in the syringe to eject a polymer jet that elongates into a nanofiber. PPFSt fibers produced at different voltages are presented in **Figure 3**. Electrospinning of PPFSt at 7 kV predominantly produces fibers with a diameter of 1.63 µm, indicating that the voltage is above the threshold. Spindle-like structures are also present among the fibers (Figure 3A). As seen in Figure 3B, raising the voltage to 10 kV improves the fiber morphology significantly since the fiber diameter reduces to 1.33 µm without droplets and spindles. A further increase in the voltage can lower the fiber diameter further to 0.95 µm. These appear inhomogeneous since some fibers become curly, likely due to an unstable polymer jet (Figure 3C).

Besides varying the voltage, the change in flow rate influences the fiber deposition rate and morphology. Increasing the flow rate for PPFSt 6 wt.% at constant voltage intuitively increases the fiber production. Yet, it also increases the diameter and ejects droplets due to the higher volume stream from the nozzle. In **Figure 4**, PPFSt 6 wt.% fibers are produced between 1.98 and 2.97 mL h^{-1}, yielding a similar fiber diameter (1.16 and 1.22 µm, respectively) and morphology. When the flow rate rises to 3.96 mL h^{-1}, from the solution, fibers are generated with diameters of 1.48 µm and, surprisingly, without droplets at the high flow rate, a high flow rate typically produces large amounts of macro droplets, making the process inefficient. Increasing the flow rate to 5.94 and 7.92 mL h^{-1} produces inhomogeneous fibers with diameters of 2.23 and 3.05 µm, respectively. Increasing the flow rate to 9.90 mL h^{-1} produces fibers with a diameter of 3.39 µm. The fibers are fused yet provide a smooth surface. This indicates that the fibers suffer from wetting as the solvent does not evaporate at this rate, causing partial dissolution and fusing.

2.4. Effect of Solution Temperature

The viscosity of the polymer solution is a function of temperature, and increasing the temperature reduces the viscosity of the polymer solution.[21] Electrospinning a polymer solution with low viscosity produces thinner fiber diameters than the solution with higher viscosity. The fibers are drawn from low solution viscosity stretch before they dry on the collector. As a result, a smaller fiber diameter is expected when electrospinning is conducted in the heated solution. **Figure 5** shows the evolution of the PPFSt fiber morphology when heated at different temperatures during the electrospinning. Heating the PPFSt solution from 25 °C to 50 °C significantly impacts the fiber diameter. This can be seen from the fiber size that decreases from 4.28 to 2.94 µm. A further increase of the temperature to 75 °C produces larger fibers with a diameter of 4.75 µm and transforms the fiber surface into smooth fibers. The increase in the PPFSt fiber diameter is attributed to the conflicting correlation between viscosity and solvent evaporation. Although viscosity decreases as the solution temperature increases, jet thinning is prevented by the rapid solvent evaporation. As soon as the solution jet is ejected, the evaporation of the solvent (THF/DMAc with 1/1 ratio) increases significantly as the solution temperature increases. Particularly at 75 °C, the THF solvent component evaporates first since its boiling point is 66 °C. It accelerates the solvent evaporation and consequently leads to a fast solidification of the fibers. This finding suggests that temperatures applied to the spun solution should not exceed the solvent's boiling point to achieve a decreased fiber diameter. In addition, the transformation of PPFSt fibers into smooth fibers at 75 °C (compared to 50 and 25 °C) is

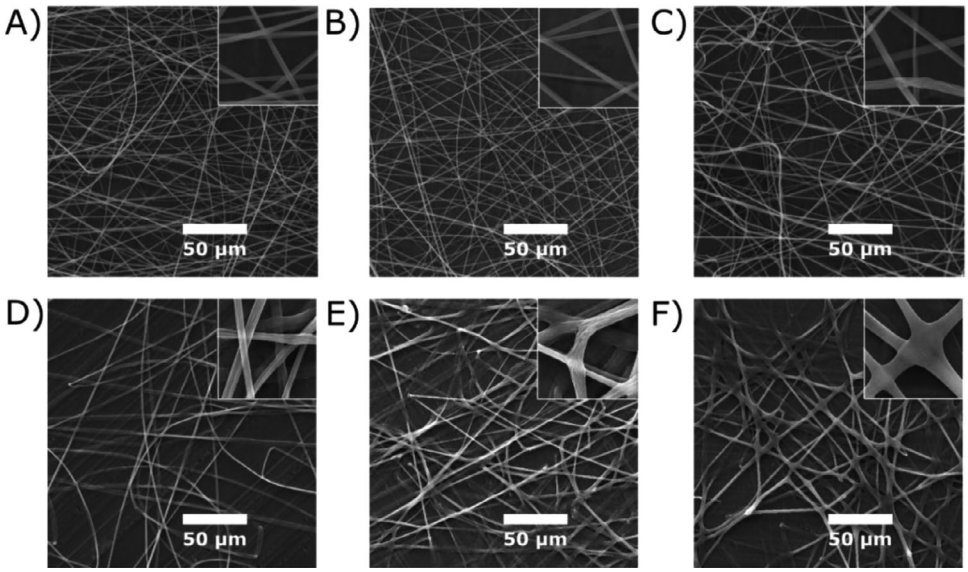

Figure 4. Effect of flow rate: A) 1.98, B) 2.97, C) 3.96, D) 5.94, E) 7.92, and F) 9.90 mL h^{-1}. The PPFSt solution is dissolved in THF/DMAc (1/1) with a concentration of 6 wt.% and electrospun at 10 kV. Inset images reflect fiber morphology at higher magnification.

attributed to the faster drying time of the polymer jet compared to its buckling time. The mechanism behind obtaining smooth or rough fiber in electrospinning has been explained by Pai et al.[22] by correlating the phenomena with buckling instabilities first described by Pauchard et al.[23] The wrinkle formation originates from the buckling of the polymer skin subjected to compressive radial stresses from solvent evaporation of the jet and due to the continuous jet elongation that simultaneously produces a lateral contraction. This occurs when the buckling time is smaller or slightly different from the drying time. During this time, conditions result in different fiber roughness. In the case of solution temperatures of 25 and 50 °C, the fibers are not smooth, indicating that the buckling time is comparable to the drying time. In contrast, smooth PPFSt fibers are produced due to further elevation of solution temperature to 75 °C, which might make the drying time much smaller than the buckling time.

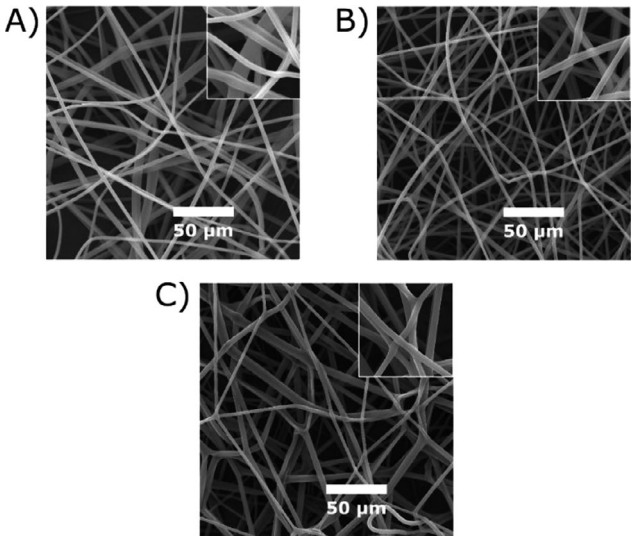

Figure 5. Effect of solution temperature on the PPFSt fiber morphology: A) 25, B) 50, C) 75 °C. The PPFSt solution is dissolved in THF/DMAc (1/1) with a concentration of 14 wt.% and electrospun at 10 kV with a flow rate of 2.73 mL h^{-1}. Inset images reflect fiber morphology at higher magnification.

2.5. Effect of Polymer Functionalization on PPFSt Fibers Morphology

The knowledge gathered from the previous results with PPFSt should be transferred to the aminated equivalents, PPFSt-TMG and PPFSt-Pip. **Figure 6** shows electrospun fibers generated from modified and unmodified PPFSt. For the unmodified PPFSt, the fiber diameter is 826 nm, while the PPFSt-Pip fibers yield diameters of 2.49 µm. Among these fibers, electrospun PPFSt-TMG provides the most minor fiber diameter with 408 nm (Figure 6C). In this case, the basicity of the fiber polymer is an essential factor that accounts for a drastic reduction in fiber diameter. The basicity of PPFSt-TMG is significantly higher than that of both unmodified PPFSt-Pip and unmodified PPFSt, which do not provide a functional group. The pK_b value of the PPFSt-Pip was calculated to have a value of 8.75, while the pK_b value of PPFSt-TMG was estimated to be 1.13 (calculated with the pK_a/pK_b module of ACD 10).

The reason for the low basicity of PPFSt-Pip is the firm –I effect of the aromatic F atoms of the tetrafluorophenyl group of PPFSt, which lowers the electron density of the lone electron pair of the N atom of the piperidine markedly. When the basicity is higher, more charges are involved in stretching the jet during the electrospinning, leading to a smaller fiber diameter.[24] Although a polymer jet contains more charges, further jet stretching is difficult to achieve if it is solidified rapidly. A significant jet thinning occurs during the whipping instability, where the jet develops into a more extensive spiral formation as the jet grows longer and thinner. Therefore, besides the effect of basicity, the

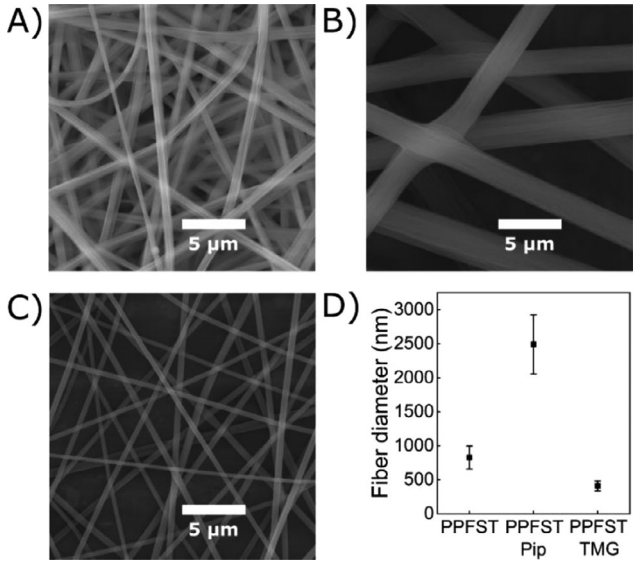

Figure 6. Effect of side chain functionalization can be seen after electrospinning of: A) unmodified, B) modified with piperidine, and C) modified with TMG. A comparison of the average fiber diameter of the unmodified and modified PPFSt is also given (D). Electrospinning of PPFSt solution or aminated PPFSt solution was carried out with a concentration of 8 wt.%, dissolved in DMAc/THF (1:1) mixture. The high voltage was kept constant at 15 kV, and the solution flow rate was set at 3.96 mL h^{-1}.

excellent solubility of PPFSt-TMG in both THF and DMAc might also be the other factor that contributes to the decrease of the fiber diameter, which allows PPFSt-TMG to retain the solvent longer during electrospinning. Since the solution jet takes longer to dry, when the polymer jet undergoes a whipping instability, the jet has a longer time to exhibit more continuous jet elongation, which thins the jet, leading to thinner solid nanofiber on the collector. Another factor that can reduce the fiber diameter is the viscosity or surface tension. However, as indicated in Figure S1 (Supporting Information), the viscosity of PPFSt-TMG is higher due to the possible hydrogen bonding. This explains that the viscosity does not influence the reduction of PPFSt-TMG nanofiber diameter.

2.6. Mechanical Properties of Aminated PPFSt Fiber-Reinforced Composite Membranes

Fiber mats can be used as membrane reinforcement in electrochemical energy devices like Nafion composite membranes. Hence, in this study, the previously fabricated fibers were infiltrated with Nafion and with, for comparison, a sulfonated aromatic and partially fluorinated polyether (SFS001), leading to dense fiber-reinforced composite membranes.

The intuitive advantage of fiber reinforcements is enhancing the membrane's mechanical strength. The mechanical properties of the Nafion composite membranes reinforced by PPFSt and aminated PPFSt at room temperature are compared with those of spray-coated Nafion without fiber reinforcement, as shown in **Figure** 7A. The Young's modulus represents the strength of the Nafion composite membrane supported by unmodified PPFSt at 489 MPa, which is an 84% increase compared to the Young's modulus of spray-coated Nafion. The yield stress, indicated by the curve before the membrane is about to deform permanently, is 8.22 MPa or an improvement of 70% compared to the non-reinforced Nafion membrane. When Nafion is reinforced by PPFSt-Pip fiber, Young's modulus and yield stress increase to 80% and 91%, respectively. PPFSt-Pip fiber mat-reinforced Nafion has a lower Young's modulus than PPFSt/Nafion composite membrane due to the larger fiber diameter, leading to lower crystallinity.[25] Although acid-base interactions can occur between PPFSt-Pip and Nafion, they are likely weak due to the low basicity of PPFSt-Pip. Unlike PPFSt-Pip/Nafion, Nafion reinforced by PPFSt-TMG nanofiber mats increases Young's Modulus and yield stress by 161% and 148%, respectively. This indicates that PPFSt-TMG provides better strength to the composite membrane than PPFSt and PPFSt-Pip.

Additionally, PPFSt fibers and aminated PPFSt fibers infiltrated with the sulfonated aromatic polymer (SFS001) are presented in Figure 7B. Here, the SFS001 reinforced by PPFSt-TMG nanofiber provides higher Young's Modulus and yield strength than the PPFSt or PPFSt-Pip equivalents. Notably, the SFS001 composite membranes yield improved mechanical strength compared to Nafion or Nafion composite membranes.

Besides the dry state, measurements of the Nafion composite membranes could also be tested in the wetted state using DMA,

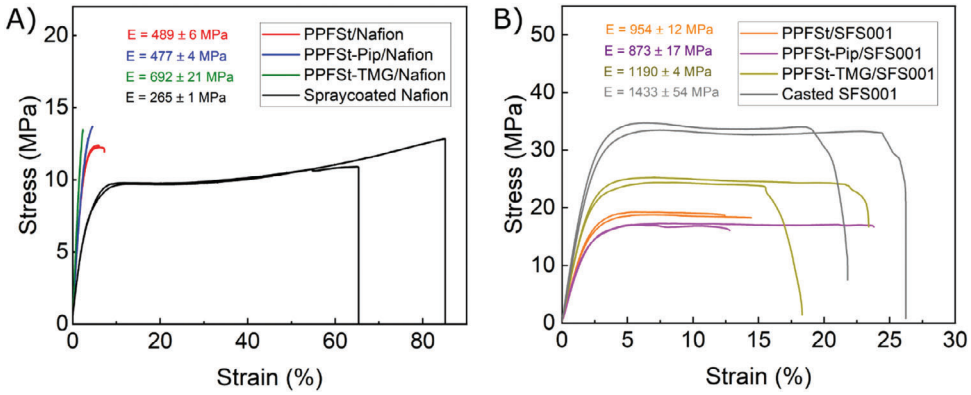

Figure 7. Tensile properties of Nafion composite membranes A) and SFS001 composite membranes B) reinforced by PPFSt and aminated-PPFSt fibers. Every sample was measured twice at room conditions (T = 24.3 °C, rH = 39%). Young's Modulus (E) represents the slopes at the beginning of stress-strain curves.

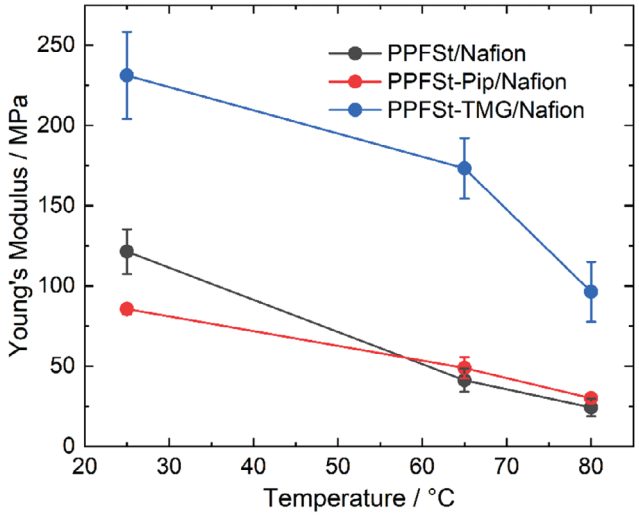

Figure 8. Young's modulus of Nafion composite membranes reinforced by PPFSt fibers and modified PPFSt containing different amino functional groups, namely tetramethyl guanidine (TMG) and piperidine (Pip). During DMA measurement, the composite membranes were immersed in a water bath at three different temperatures (25, 65, and 80 °C).

which is vital for their application in electrochemical devices such as redox flow batteries and electrolyzers. The DMA measurement in a wetted state is not reasonable for pristine SFS001 membranes and their composite membranes due to excessive swelling. **Figure 8** depicts the Young's Modulus of hydrated composite membranes. The fibers (PPFSt, PPFSt-Pip, and PPFSt-TMG) are rather hydrophobic, so the Nafion polymer softens by incorporating water into the membrane. In addition, the temperature influences the Young's modulus of the composite, where increasing the temperature reduces the Young's Modulus. However, the Young's Modulus of PPFSt fiber-reinforced membrane at 80 °C is improved compared to a pristine Nafion membrane.[10] The Young's modulus of PPFSt/Nafion and PPFSt-Pip/Nafion are comparable in the wet state and high temperature, while PPFSt-TMG/Nafion yields the highest Young's modulus.

2.7. Proton Conductivity of the Ionomer-Filled Fiber Mat Composite Membranes

Besides the mechanical properties, proton conductivity is a crucial property directly affecting the performance of electrochemical devices such as fuel cells, electrolyzers, and redox flow batteries. The proton conductivities at room temperature and water uptake of Nafion and SFS001 reinforced with PPFSt fibers and aminated PPFSt fibers are presented in **Table 2**. Both Nafion and SFS001 contain comparable fiber mat densities, yet the SFS001 composite membranes are slightly thicker than the Nafion composite membranes. As highlighted, electrolyte and water uptake are major points since a dehydrated membrane would exhibit poor proton conductivity. When the electrolyte and water uptake of the membrane is high, the membrane shows a high proton conductivity due to a higher number of connected proton transport channels. This is particularly valid for SFS001, which has a high water uptake of almost 1500%. Here, the SFS001-filled fiber composite membranes show a substantial reduction in water uptake from 79% to 84%, compared to pure SFS001, as the fiber mat reinforcements limit intense swelling. For the Nafion composites, the opposite is the case. Here, the composites show a double water uptake of ≈ 40%, compared to neat Nafion, which can be explained by voids or free volumes at the interface between fiber and matrix. The voids can be filled with water, resulting in higher water uptake of the Nafion composite membranes.

For PPFSt/Nafion, the incompatibility between hydrophobic fiber and hydrophilic Nafion could create free volumes at the interface. The effect of the aminated PPFSt fiber mat can be seen in the protonic conductivity of PPFSt-TMG/Nafion, which achieves 23 ± 1 mS cm^{-1}. The value is much lower than PPFSt/Nafion and PPFSt-Pip/Nafion, which achieve 39 ± 1 and 67 ± 2 mS cm^{-1}, respectively. This indicates the stronger basicity of PPFSt-TMG compared to PPFSt-Pip, lowering the concentration of free protons in the membrane by acid-base interactions between the PPFSt-TMG nanofibers and the Nafion matrix. Interestingly, although PPFt-Pip has a low basicity, PPFSt-Pip/Nafion has higher protonic conductivity than PPFSt/Nafion, which might be due to its larger fiber diameter that reinforces Nafion compared to PPFSt fiber, leading to better percolation pathways within Nafion.

Table 2. Ex situ proton conductivity and water uptake measurements of Nafion and SFS001 composite membranes with three different types of fiber reinforcement (PPFSt fiber, PPFSt-Pip fiber, and PPFSt-TMG fiber) by electrical impedance spectroscopy. The measurement was carried out at room temperature using 0.5 M H_2SO_4 as an electrolyte to reduce contact resistance.

Membrane types	Fiber density [mg cm^{-2}]	Fiber Mass Fraction [%]	Membrane thickness [µm]	Protonic conductivity [mScm^{-1}]	IEC [meq. g^{-1}]	Water uptake [%]
PPFSt/Nafion composite	0.63	14.2	26	39 ± 1	0.84 ± 0.07	40 ± 10
PPFSt-Pip/Nafion composite	0.67	15.5	26	67 ± 2	0.79 ± 0.2	43 ± 10
PPFSt-TMG/Nafion composite	0.67	14.7	26	23 ± 1	0.78 ± 0.1	42 ± 14
Nafion 212	–	–	51	80 ± 2	0.95-1.03**	10.5[26]
Spray-coated Nafion D2020	–	–	32	116 ± 8*	1.02 ± 0.02	21 ± 6
PPFSt/SFS001 composite	0.66	13.1	48	40 ± 2	2.02 ± 0.2	236 ± 25
PPFSt-Pip/SFS001 composite	0.63	15.8	48	64 ± 4	2.05 ± 0.15	299 ± 15
PPFSt-TMG/SFS001 composite	0.66	10.6	53	56 ± 2	1.97 ± 0.06	223 ± 7
SFS001	–	–	57	127 ± 4*	2.2 ± 0.05	1448 ± 21

Note: *the spray-coated Nafion and SFS001 values differ drastically due to higher H_2SO_4 uptake. ** values provided by the supplier.

Another factor for the higher proton conductivity of PPFSt-Pip/Nafion composite membranes, compared to PPFSt/Nafion composite membrane, might be the reduced hydrophobicity of them (PPFSt-Pip has 4 F atoms in its repeat unit, while pure PPFSt has 5 F atoms). Compared to pure (non-reinforced) Nafion membranes, in which the proton conductivities are 80 ± 2 mS cm^{-1} for commercial Nafion 212 and 116 ± 8 mS cm^{-1} for the spray-coated Nafion, the protonic conductivities of the Nafion composite membrane are lower, which explains the influence of the non-conducting fiber mat supporting the Nafion matrix. Acid-base interactions also occur in the SFS001 composite membranes since SFS001 contains sulfonic acid groups. Infiltrating the fiber mat with SFS001 leads to composite membranes with higher proton conductivity than the Nafion composite membranes investigated in this study. In PPFSt/SFS001, the fiber mat has zero ionic charge, resulting in improved proton conductivity of 40 ± 2 mS cm^{-1} compared to that of PPFSt-Pip/SFS001 and PPFSt-TMG/SFS001 that reach 64 ± 4 and 56 ± 2 mS cm^{-1}, respectively. When the proton conductivity of PPFSt/SFS001 is compared to PPFSt/Nafion, SFS001 is more conductive than Nafion, which is correlated to the significantly higher IEC of SFS001 of 2.2 mequiv. g^{-1}. The IEC is reduced when acid-base interactions within the SFS001 composite membrane exist. This is also reflected in a lower IEC beyond the reduction by the mass fraction of fibers in all membranes. However, those of the sulfonic acid groups that do not interact with the amino groups of the fiber mat PPFSt polymers lead to the observed high proton conductivity of the SFS-filled composite membranes.

A comparison of the conductivities for similar reinforced membranes for redox flow battery applications is delicate as testing protocols vary strongly in literature. Already, measurement of commercial Nafion 212 can result in different conductivity values from 63 mS cm^{-1} (measured in 0.5 M H_2SO_4) to 43.2 mS cm^{-1} (measured in 3 M H_2SO_4) to 71 mS cm^{-1} (measured in water).[13,27] This renders the internal standard more important as values may not be comparable due to different instrumental setups. Taking the internal standard of 43.2 mS cm^{-1}, the developed reinforced PBI-Nafion membrane provided a conductivity of 24.2 mS cm^{-1} in 3 M H_2SO_4, In these studies, the reinforced membranes show inferior conductivity compared to Nafion, however a strong reduction of ion cross-over can be achieved by implementation of the fiber mats.

3. Conclusion

In conclusion, the fabrication of electrospun modifiable PPFSt nanofibers was investigated in depth to screen for a novel aminated fiber material as a possible alternative to poly(benzimidazole) fibers. The solvent, polymer concentration, voltage, flow rate, and temperature parameters were varied. Adding a high boiling point solvent (DMAc or DMSO) into PPFSt/THF favored the formation of smooth nanofibers without spindle-like structures. From varying PPFSt concentrations from 2 wt.% to 20 wt.%, electrospinning yields beadless nanofibers at 4 wt.% and 8 wt %, with diameters of 0.73 and 1.3 µm, respectively. Changing the electrospinning voltage changes the fiber quality, where the voltage of 10 kV results in more uniform fibers compared to that of 7 and 15 kV. Increasing the solution temperature from 25 to 50 °C reduces the fiber diameter, but raising the temperature further to 75 °C creates a larger fiber diameter, likely due to the fast evaporation of the low boiling point solvent used under these conditions. A flow rate as high as 3.96 mL h^{-1} can be reached before producing large fibers with diameters above 5 µm and fused fibers. Those parameters, except the temperature, were adopted to produce tetramethylguanidine and piperidine-modified PPFSt fibers. Due to the high basicity, PPFSt-TMG produced nanofibers with a diameter of 408 nm, much smaller than 2.49 µm for PPFSt-Pip under equal conditions. Infiltrating the fibers with Nafion and SFS001 provides better compatibility when more alkaline fibers exhibit acid-base interactions with sulfonic acid groups from the matrix.

Consequently, the PPFSt-TMG/Nafion showed a higher mechanical strength than PPFSt-Pip/Nafion and PPFSt/Nafion. Additionally, the interactions decrease proton conductivity from 67 mS cm^{-1} for the PPFSt-Pip/Nafion to 23 mS cm^{-1} for the PPFSt-TMG/Nafion. Similarly, for SFS001 equivalents, the PPFSt-Pip/SFS001 outperformed PPFSt-TMG/SFS001 by a difference of 12 mS cm^{-1}. Here, the swelling is reduced remarkably to almost sevenfold. These findings give access to a sweet spot for a reasonable pK^b value of fiber material, balancing fiber-matrix integrity and proton conductivity. In ongoing studies, as possible, further basic polymers will be studied, such as electrospun nanofiber reinforcements for proton-conducting membranes applied to electrochemical applications such as fuel cells, electrolyzers, and redox-flow batteries.

4. Experimental Section

Materials: Tetrahydrofuran (THF), N, N-dimethylacetamide (DMAc; anhydrous, 99.8%), dimethyl sulfoxide (DMSO), acetone, tetramethylguanidine, piperidine, potassium peroxydisulfate and sodiumdodecylsulfate, monosodium phosphate were purchased from Sigma Aldrich. Pentafluorostyrene was purchased from Manchester Organics without a stabilizing agent. Nafion D2020 and Nafion N212 were purchased from Ion Power. SFS001 was purchased from Riva.[16]

Polymer Synthesis—Polypentafluorostyrene (PPFSt) synthesis: PPFSt was synthesized according to the literature.[28] Sodium dodecyl sulfate (2.5 g, 8.6 mmol) and monosodium phosphate (0.125 g, 1.1 mmol) were dissolved in degassed water (250 ml). Potassium peroxydisulfate (0.55 g, 2.3 mmol) was added and stirred until completely dissolved. Pentafluorostyrene (125 g, 0.64 mol) was added at vigorous stirring, leading to a homogeneous emulsion. The emulsion was filled into microwave vessels, and the reaction was executed in the microwave at a constant temperature of T = 90 °C for 2 h. The mixture was precipitated in an isopropanol-water mixture (1:1 v/v). The solid was filtered, washed with isopropanol and water, and dried in a vacuum oven at 80 °C for two days. The yield (white powder) was 110 g (88%). Molecular weight and molecular weight distribution of PPFSt were measured in THF using an Agilent GPC/SEC with polystyrene standards.

$$^1H - NMR\ (in\ d8 - THF) : \delta = 2\ ppm, 2.5\ ppm, 2.8\ ppm$$

$$^{19}F - NMR\ (in\ d8 - THF) : \delta = -144\ ppm, -158\ ppm, -165\ ppm$$

$$GPC : M_n = 156\ kDa, M_w = 524\ kDa$$

PPFSt-TMG Synthesis: To prepare PPFSt-TMG in the CEM Discover 2.0 microwave reactor (MR), 1 g PPFSt and 20 ml DMAc were filled into a 35 ml vessel. While stirring, the mixture was heated to 120 °C in the microwave for over 30 min so that PPFSt was dissolved. Then argon was bubbled through the mixture for 5 – 10 min. Subsequently, TMG was added in excess at 2.97 g (3.2283 ml). The reaction occured under stirring in the

Table 3. Elemental analysis of PPFSt-TMG.

Element	Determined amount [%]	Calculated amount [%]
C	53.635	55.4
H	5.340	5.65
N	13.655	13.85

microwave for 7 h at 150 °C. The polymer was precipitated dropwise in water, washed, and dried at 60 °C for 24 h.

$^{1}H - NMR\ (in\ CDCl_3) : \delta = 1.9\ ppm, 2.7\ ppm$

$^{19}F - NMR\ (in\ CDCl_3) : \delta = -157\ ppm, -152\ ppm, -146\ ppm$

All fluorine peaks are shifted in comparison to PPFSt. However, the determination of the degree of functionalization with TMG is not possible by integrating the para-peak due to merging peaks by a partial protonation of the PPFSt-TMG. The following elemental analysis confirms the synthesis of PPFSt with 100% TMG-functionalization (**Table 3**).

For the analysis of the FTIR spectra, the broad band at the wave number range of 2973 ± 1 cm^{-1} is associated with CH_3-groups, and the band at 1148 ± 1 cm^{-1} corresponds to the stretching vibration C-N of the amine. These indicate the functionalization of PPFSt with TMG.

PPFSt-Pip Synthesis: PPFSt-Pip was synthesized similarly to PPFSt-TMG. 5 g (25.75 mmol) of PPFSt were dissolved in 20 ml DMAc at 120 °C. After cooling the solutions to room temperature, 12.59 ml piperidine (Pip) (128.75 mmol) was added to the reaction solution under argon. The reaction was stirred at 150 °C for 7 h. For the purification of the PPFSt-Pip polymer, the hot polymer solution was precipitated in water. The resulting white product was washed several times with ethanol and dried at 75 °C for 24 h.

$^{1}H - NMR\ (in\ CDCl_3) : \delta = 1.6\ ppm, 1.9\ ppm, 2.4\ ppm, 2.6\ ppm, 3.1\ ppm$

$^{19}F - NMR\ (in\ CDCl_3) : \delta = -146\ ppm, -151\ ppm$

The complete functionalization with TMG was controlled with ^{19}F NMR by the disappearance of the peak at $\delta = -165$ ppm, which equals the two fluorine atoms from PPFSt, and the presence of the peak $\delta = -146$ ppm, which equals two fluorine atoms PPFSt-TMG. The degree of functionalization was determined as 100%.

Electrospinning of Polymers—Electrospinning Method: Electrospun fibers were produced by a KATO TECH electrospinning unit (made in Japan) and schematically depicted in **Figure 9**. The setup includes a high-voltage system, a syringe pump, a metal nozzle, and a metal collector. The fiber properties, such as structure, diameter, porosity, and orientation, are affected by electrospinning parameters, which are divided into solution, operational, and environmental parameters. In this case, only selected parameters were used that are assumed to affect the fiber morphology, such as solvent, polymer concentration, voltage, flow rate, and temperature of the solution. Before electrospinning, acetone, THF, DMAc, and DMSO were selected to dissolve PPFSt. The properties of those solvents are depicted in Table S1 (Supporting Information). PPFSt solutions were prepared in different concentrations. During electrospinning, PPFSt solution is contained in a 20 mL syringe and extruded through a metal nozzle (inner diameter of 0.5 mm) connected with varied voltages and flow rates. A PPFSt solution was applied by various voltages with the same flow rate to investigate the effect of voltage. To examine the impact of flow rate on the PPFSt fiber, the flow rate of the PPFSt solution was also varied at a fixed voltage. For varying solution temperatures, the setup was based on the previous work,[15] in which a metal syringe jacket connected to an external heat exchanger is used to heat the 10 mL syringe containing PPFSt solution at three different temperatures (25, 50, 75 °C). A larger nozzle with an inner diameter of 0.8 mm was used if the polymer solution dried quickly and clogged the nozzle. In addition to electrospinning of unmodified PPFSt, aminated PPFSt nanofibers were also electrospun by using the same parameters as for the unmodified PPFSt to see the effect of the amine functional groups on the produced nanofibers. The distance between the nozzle and collector was 20 cm for all electrospinning experiments.

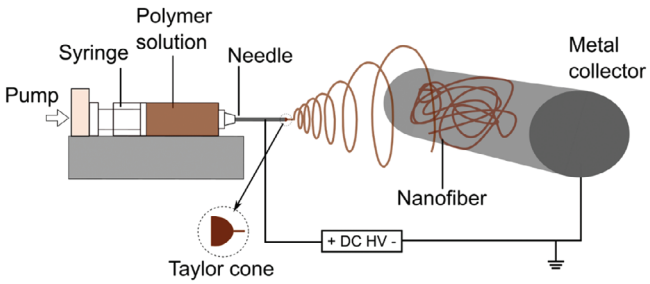

Figure 9. Conventional electrospinning setup with a polymer solution-filled syringe and a needle to extrude the charged polymer solution to the collector.

Preparation of Composite Membranes from PPFSt, the Modified PPFSt Polymers, and Nafion/SFS: In this study, two types of proton exchange membranes, namely Nafion (D2020) and sulfonated partially fluorinated polymer (SFS001), were reinforced by unmodified PPFSt and aminated PPFSt fibers. Due to the different behavior between Nafion and SFS001 solutions, the composite membranes were prepared separately by two methods, illustrated in Scheme 1. Applying the first method (Scheme 1A), the composite membranes were produced by pore-filling the electrospun fiber mat produced from PPFSt and its modifications via spray-coating. For the Nafion composite membranes, an ultrasonic spray-coater (Sono-Tek, USA) was used to create a Nafion layer into a PTFE substrate by applying the following parameters: flow rate of 0.8 mL $mi^{-1}n$, nozzle speed of 100 mm s^{-1} with eight runs, shaping air of 0.2 kPa, ultrasonic power of 3 W, and substrate temperature of 25 °C. Nafion, including the substrate, was attached to the aluminum collector. Fiber reinforcement, either PPFSt or aminated PPFSt fiber, was deposited on the Nafion layer by electrospinning of PPFSt solution or aminated PPFSt solution with a concentration of 8 wt.%, dissolved in DMAc/THF (1:1) mixture. During electrospinning, a high voltage was kept constant at 15 kV from the nozzle to the collector that was separated at 20 cm, and the solution flow rate was set at 3.96 mL h^{-1}. The area density of the fibers was determined by weighing a specific size of the spun fiber mat after electrospinning. The top layer was sprayed with Nafion (10 runs) to fill the fiber mat voids, resulting in dense fiber-reinforced Nafion composite membranes. The SFS001 composite membranes were prepared based on the second method depicted in Scheme 1B. An SFS001 solution dissolved in isopropanol with a concentration of 20 wt % was cast on a PTFE substrate at room temperature. The height of the movable blade from the substrate was adjusted to 100 µm. After drying the SFS001 layer for 1 h, the unmodified PPFSt and aminated-PPFSt nanofibers were deposited onto the SFS001 layer in the electrospinning device by employing the same parameters described in the first method. SFS001 solution was cast again with substrate-blade gap at 300 µm for five times to fill the fiber mat voids and complete the production of fiber-reinforced SFS001 composite membranes. The composite membranes were detached from the substrate and characterized.

Characterization of Polymers and Fibers—NMR Spectroscopy: NMR-spectroscopy was performed at RT with a JNM-ECZ500R 500 MHz FT NMR spectrometer from JOEL (Germany) GmbH.

Gel Permeation Chromatography (GPC): The number of average molecular weight (M_n) and polydispersity (PDI) were determined by SEC with a SECcurity^2 1260 from PSS equipped with one PSS SDV LUX GUARD, one PSS SDV LUX 3 µm 1000 Å and two PSS SDV LUX 3 µm 10 000 Å. THF at 35 °C and NMP with 1 g mL^{-1} LiBr were used as eluent and Polystyrene as standard.

Differential Scanning Calorimetry (DSC): DSC measurements were carried out on a STARe DSC 3+ from Mettler Toledo with 10 K min^{-1} in

50 mL min^{-1} N_2. Two heating and one cooling segment were recorded. If the start temperature is below RT, a 5-min isotherm was used beforehand. The Richardson method determines the glass transition temperature (T_g) and is averaged from the cooling and second heating curves. TGA measurements were performed on a TGA 8000 from PerkinElmer Inc. with 10 K min^{-1} in 30 mL min^{-1} synthetic air. Heating was carried out from 30-800 °C.

Scanning Electron Microscopy (SEM) of Nanofibers: The morphology of electrospun nanofiber meshes was investigated using a scanning electron microscope (SEM) imaged at an accelerating voltage of 20 kV. A small as-spun fiber mat sample was taken from the electrospinning collector utilizing a scalpel and put on carbon tape, previously attached to a metal holder. Due to the low electrical conductivity of samples, gold sputtering was performed on the samples before imaging to avoid charging artifacts.

Characterization of Composite Membranes—Tensile Test: The strength of the composite membranes was measured in a tensile tester (EZ-SX, SHIMADZU Corporation, Japan) at room temperature (T = 23.9 °C, rH = 39%). The thicknesses of Nafion composite membranes were ≈ 26 µm, while SFS001 composite membranes ranged from 46 – 52 µm, as determined by a micrometer gauge. A 1 cm x 4 cm rectangular area was cut from the membrane and put between two metal grips. A tensile test was performed by stretching the membrane at a constant speed of 5 mm min^{-1}. The modulus of elasticity results from the stress-strain ratio in the elastic region, which can be calculated by

$$E = \frac{\Delta\sigma}{\Delta\epsilon} \tag{1}$$

where E is the elastic modulus, while σ and ϵ represent stress and strain, respectively. Yield stress represents the boundary between the elastic and plastic region of the stress-strain curve and is determined by dragging the elastic slope to 0.2% strain offset for all membrane samples. The yield point intersects the slope line and the stress-strain curve.

Dynamic Mechanical Analysis (DMA): Dynamic mechanic analysis measurements were performed using the DMA 1 from Mettler Toledo, equipped with tensile mode. All membranes were immersed in deionized water for 24 h before testing and analyzed at 25 °C in a water bath with a preload force of 0.5 N, a force rate of 1 N min^{-1}, and an upper force limit of 12 N. The composite membranes were hydrated in a water bath at three different temperatures (25, 65, and 80 °C)

Conductivity: Through-plane conductivities were measured by the electrochemical impedance spectroscopy method over the frequency range 1 kHz–10 MHz at RT with an AC impedance technique using an electrochemical workstation Zennium X of Zahner equipped with a separate conductivity cell. As an electrolyte, 0.5 M H_2SO_4 was used. The proton conductivities of the membranes were calculated by

$$\sigma = \frac{L}{R \times A} \tag{2}$$

where σ is defined as the reciprocal of R with the unit Siemens per centimeter [S cm^{-1}]. R is the resistance [Ohm], L is the membrane thickness [cm], and A is the area of the gold electrodes [0.25 cm^2]. The proton conductivity values were collected for three measurements and averaged.

Water Uptake: The water uptake (WU) of the membranes in percent was calculated according to the Equation (3).

$$WU = \left(\frac{m_{wet} - m_{dry}}{m_{dry}}\right) \times 100\% \tag{3}$$

where m_{wet} and m_{dry} represent the mass of wet membranes and the mass of dry membranes, respectively, the membranes were put in water for one day at 80 °C. To weigh the wetted membrane, the excess water was wiped off gently with a tissue to remove superficial water. The water uptake values were obtained from three individual measurements.

Supporting Information

Supporting Information is available from the Wiley Online Library or from the author.

Acknowledgements

The authors gratefully acknowledge financial support from the Deutsche Forschungsgemeinschaft (DFG). In addition, Mr. Mu'min would like to thank the Indonesia Endowment Fund for Education (LPDP) for their support (October 2017 – March 2022).

Conflict of Interest

The authors declare no conflict of interest.

Data Availability Statement

The data that support the findings of this study are available in the supplementary material of this article.

Keywords

composite membrane, electrospinning, nanofibers, polymer functionalization, proton exchange membrane

Received: July 8, 2024
Revised: September 27, 2024
Published online: October 29, 2024

[1] L. Lou, O. Osemwegie, S. S. Ramkumar, *Ind. Eng. Chem. Res.* **2020**, *59*, 5439.
[2] C. S. Gittleman, A. Kongkanand, D. Masten, W. Gu, *Curr. Opin. Electrochem.* **2019**, *18*, 81.
[3] P. Gibson, H. Schreuder-Gibson, D. Rivin, *Colloids Surf. A* **2001**, *187–188*, 469.
[4] X. Gong, G. He, Y. Wu, S. Zhang, B. Chen, Y. Dai, X. Wu, *J. Power Sources* **2017**, *358*, 134.
[5] Y. Huang, J. Song, C. Yang, Y. Long, H. Wu, *Mater. Today* **2019**, *28*, 98.
[6] L. Hou, N. Wang, J. Wu, Z. Cui, L. Jiang, Y. Zhao, *Adv. Funct. Mater.* **2018**, *28*, 1801114.
[7] G. Wang, D. Yu, A. D. Kelkar, L. Zhang, *Prog. Polym. Sci.* **2017**, *75*, 73.
[8] S. Megelski, J. S. Stephens, D. B. Chase, J. F. Rabolt, *Macromolecules* **2002**, *35*, 8456.
[9] G. Collins, J. Federici, Y. Imura, L. H. Catalani, *J. Appl. Phys.* **2012**, *111*, 44701.
[10] M. S. Mu'min, M. Komma, D. Abbas, M. Wagner, A. Krieger, S. Thiele, T. Böhm, J. Kerres, *J. Membr. Sci.* **2023**, *685*, 121915.
[11] a) J. Kerres, A. Ullrich, F. Meier, H. Thomas, *Solid State Ionics* **1999**, *125*, 243; b) J. A. Kerres, *J. Membr. Sci.* **2001**, *185*, 3;
[12] R. Sood, S. Cavaliere, D. J. Jones, J. Rozière, *Nano Energy* **2016**, *26*, 729.
[13] Y. H. Wan, J. Sun, Q. P. Jian, X. Z. Fan, T. S. Zhao, *J. Mater. Chem. A.* **2022**, *10*, 13021.
[14] a) O. Zholobko, X.-F. Wu, Z. Zhou, T. Aulich, J. Thakare, J. Hurley, *J. Appl. Polym. Sci.* **2020**, *137*, 49639; b) M. Najibah, E. Tsoy, H. Khalid, Y. Chen, Q. Li, C. Bae, J. Hnát, M. Plevová, K. Bouzek, J. H. Jang, H. S. Park, D. Henkensmeier, *J. Membr. Sci.* **2021**, *640*, 119832;

[15] D. Abbas, M. S. Mu'min, M. Bonanno, S. Thiele, T. Böhm, *J. Appl. Polym. Sci.* **2022**, *139*, e52730.
[16] F. Schönberger, J. Kerres, *J. Polym. Sci. A Polym. Chem.* **2007**, *45*, 5237.
[17] V. Atanasov, J. Kerres, *Macromolecules* **2011**, *44*, 6416.
[18] A. Haider, S. Haider, I.-K. Kang, *Arabian J. Chem.* **2018**, *11*, 1165.
[19] J. Xue, T. Wu, Y. Dai, Y. Xia, *Chem. Rev.* **2019**, *119*, 5298.
[20] S. I. Tamim, J. B. Bostwick, *Soft Matter* **2021**, *17*, 4170.
[21] C. Mituppatham, M. Nithitanakul, P. Supaphol, *Macromol. Chem. Phys.* **2004**, *205*, 2327.
[22] C.-L. Pai, M. C. Boyce, G. C. Rutledge, *Macromolecules* **2009**, *42*, 2102.
[23] L. Pauchard, J.-P. Hulin, C. Allain, *Europhys. News* **2005**, *36*, 9.
[24] C. J. Angammana, S. H. Jayaram, *IEEE Trans. on Ind. Appl.* **2011**, *47*, 1109.
[25] A. Baji, Y.-W. Mai, S.-C. Wong, M. Abtahi, P. Chen, *Compos. Sci. Technol.* **2010**, *70*, 703.
[26] C. Feng, Y. Li, K. Qu, Z. Zhang, P. He, *RSC Adv.* **2019**, *9*, 9594.
[27] a) G. Palanisamy, T. Sadhasivam, W.-S. Park, S. T. Bae, S.-H. Roh, H.-Y. Jung, *ACS Sustainable Chem. Eng.* **2020**, *8*, 2040; b) C. Jeon, C. Choi, H.-T. Kim, M. Seo, *ACS Appl. Energy Mater.* **2020**, *3*, 5874;
[28] V. Atanasov, M. Bürger, S. Lyonnard, L. Porcar, J. Kerres, *Solid State Ionics* **2013**, *252*, 75.

